ISSN 2616-5767 Vol.7, Issue 4: 84-92, DOI: 10.25236/AJETS.2024.070413

Cross-Condition Intelligent Fault Diagnosis of Rolling Bearing Based on Rationle-Invariant Domain Adversarial Networks

Zhichao Zhou[1,2], Chaofan Hu[1,2,*]

[1]*School of Mechanical and Electrical Engineering, Guilin University of Electronic Technology, 541004, Guilin, China*
[2]*Guangxi Key Laboratory of Manufacturing System & Advanced Manufacturing Technology, Guilin University of Electronic Technology, 541004, Guilin, China*
**Corresponding author*

Abstract: *Our study introduces an innovative intelligent fault diagnosis approach employing the Rationale Invariance-Domain Adversarial Network (RIDAN). This approach leverages domain generalization principles to enhance classification accuracy for data from unknown target domains. The process begins by transforming one-dimensional bearing vibration signals, captured through acceleration sensors, into two-dimensional gray pixel images. Subsequently, a domain discriminator is developed to learn domain-specific features and align domain distributions. Concurrently, a label classifier is established, incorporating rationale matrices for different categories. Our research rigorously validates this methodology using datasets from Guilin University of Electronic Technology and Case Western Reserve University. When compared with contemporary domain generalization methods, our approach shows excellent efficacy in bearing fault diagnosis across different operating domains.*

Keywords: *rolling bearings; intelligent fault diagnosis; domain adversarial neural networks; rationale invariance; domain generalization*

1. Introduction

The swift advancement of the modern intelligent manufacturing industry has propelled rotating machinery within industrial equipment toward a new era of intelligence and ultra-precision. This evolution is not only a catalyst for technological innovation but also establishes elevated standards for the safety and stability of rotating machinery [1-3]. Rotating machinery plays a pivotal role in numerous sectors, including aerospace, transportation, medical devices, and clean energy, proving to be an essential component of mechanical systems. Bearings, as a crucial element of rotating machinery, significantly influence the operational safety of the entire system [4]. These bearings operate under extremely harsh conditions, bearing the responsibility of supporting rotation while often enduring complex forces such as shock loads and alternating loads. Consequently, they are among the most failure-prone components in equipment. The early detection and prompt addressing of faults in bearings are imperative. Neglect in this regard can lead to not only equipment degradation but also pose substantial risks to personal safety [5-6]. Despite the industry's widespread acknowledgment of the criticality of bearing fault diagnosis, discovering an efficient and reliable method for fault detection remains a formidable challenge that urgently demands a solution.

Traditional fault diagnosis methods predominantly rely on signal processing and fault mechanism models. In these methods, researchers utilize signal processing techniques to analyze bearing vibration signals. This analysis enables them to extract characteristic fault indicators and ascertain the health status of the bearings [2]. Given the typically non-smooth and non-linear nature of bearing vibration signals, the application of time-frequency analysis methods capable of handling such complexities becomes crucial[7]. Prominent time-frequency analysis methods include wavelet transform[8], Fourier transform[9], empirical mode decomposition[10], and the Hilbert-Huang transform[11]. These traditional methods offer an intuitive reflection of signal changes, enabling the use of bearing fault characteristic frequencies for precise fault localization. They are particularly adept at handling non-smooth and non-linear signals. However, the limitations of these methods are also evident. They require complex preprocessing steps like filtering, noise reduction, and decomposition. Moreover, the interpretation and judgment of the time-frequency

ISSN 2616-5767 Vol.7, Issue 4: 84-92, DOI: 10.25236/AJETS.2024.070413

diagrams heavily depend on expert knowledge and experience. This reliance on manual expertise falls short of meeting the increasing demands for 'intelligent' in modern diagnostic approaches.

2. Domain generalization in fault diagnosis

In recent times, the realm of domain generalization has emerged as a focal point of research, particularly due to the challenge posed by the inaccessibility of target domain data. There is often confusion between domain generalization and domain adaptation methods, though both fall under the umbrella of generalized transfer learning, they possess distinct characteristics. The fundamental difference lies in the accessibility of target domain data during network training. Domain adaptation methods have the advantage of accessing target domain data (whether labeled or unlabeled) during training. In contrast, domain generalization methods operate under the constraint of having no access to target domain data throughout the training phase[12]. This distinction sets domain generalization apart from traditional machine learning, deep learning, and narrow transfer learning approaches.

Table 1 succinctly outlines the distinctions among the four methodologies. Domain generalization methods, in comparison to the others, operate under more rigorous conditions. They exclusively permit model training within the source domain, entirely excluding target domain data from the training process. Consequently, domain generalization can be perceived as an advanced iteration of the domain adaptation approach. It embodies a heightened level of complexity and challenge, aiming to tackle more intricate issues related to data access and the alignment of data distributions. This evolution marks a significant leap in the field, pushing the boundaries of what can be achieved in model training and application in varied domain settings.

Table 1:Differences among Methods.

Methodology	Target domain data	Training set	Test set	condition
Traditional ML/DL	available, labeled	D	D	I.I.D condition
Transfer learning	available, unlabeled/ labeled	$D_s,\ D_t$	D_t	$Y_s \neq Y_t$
Domain adaptation	available, unlabeled/ labeled	$D_s,\ D_t$	D_t	$P(X_s) \neq P(X_t)$
Domain generalization	unavailable	$D_1, \ldots,\ D_n$	D_{n+1}	$P(D_i) \neq P(D_j), 1 \leq i \neq j \leq n+1$

The ultimate goal of domain generalization is to train a prediction function $h\colon \mathrm{X} \to \mathrm{Y}$ with strong generalization ability on multiple known source domain datasets such that it minimizes the error on the target domain D_t , i.e.:

$$\min_h \mathrm{E}_{(x,y)\in D_t}\left[\ell\left(h\left(x\right),y\right)\right] \tag{1}$$

where E and $\ell\left(\cdot,\cdot\right)$ are the expectation and loss functions, respectively.

During the training process, DANN has two goals: one is to minimize the classification error of the label classifier G_y on the source domain, and the other is to maximize the domain discriminative error of the domain discriminator G_d on both the source and target domains. This approach allows the feature distributions of different domains to be as consistent as possible, and if the domain discriminator is unable to discriminate between features in the source and target domains, then it means that the feature extractor G_f learns domain-invariant features that are more conducive to the generalization of the label classifier G_y over the target domain. DANN adds a domain discriminator with a gradient reversal layer (GRL) after the feature extractor. The gradient reversal layer (GRL) does not change the feature vector f during forward propagation but multiplies the gradient of the domain discriminator G_d to the feature extractor G_f by a negative number λ during backpropagation, which serves to reduce the feature extractor's sensitivity to domain-specific features.

Suppose there exists a sample space X and a corresponding label space Y = {0, 1, ..., L-1}. There exists a domain space D containing several source domains D_S^K and a target domain D_T with

ISSN 2616-5767 Vol.7, Issue 4: 84-92, DOI: 10.25236/AJETS.2024.070413

different domain distributions. The k-th source domain is denoted as $D_S^k = \left\{\left(x_i^k, y_i^k\right)\right\}_{i=1}^{n^k}$, where n^k denotes the number of samples possessed by the kth source domain, and the total number of source domain samples is $n = \sum_{k=1}^{K} n^k$. Similarly, the unlabeled target domain is denoted by $D_T = \{x_i\}_{N-n}^{N}$ and the total number of all samples is $N = n + n'$.

The prediction loss and domain loss of DANN are denoted as respectively:

$$\mathcal{L}_y^i(\theta_f, \theta_y) = \mathcal{L}_y(G_y(G_f(\mathbf{x}_i; \theta_f); \theta_y), y_i), \tag{2}$$

$$\mathcal{L}_d^i(\theta_f, \theta_d) = \mathcal{L}_d(G_d(G_f(\mathbf{x}_i; \theta_f); \theta_d), d_i) \tag{3}$$

The DANN network is then trained by optimizing the objective function E to obtain the optimal parameters:

$$E(\theta_f, \theta_y, \theta_d) = \frac{1}{n}\sum_{i=1}^{n}\mathcal{L}_y^i(\theta_f, \theta_y) - \lambda\left(\frac{1}{n}\sum_{i=1}^{n}\mathcal{L}_d^i(\theta_f, \theta_d) + \frac{1}{n'}\sum_{i=n+1}^{N}\mathcal{L}_d^i(\theta_f, \theta_d)\right). \tag{4}$$

Maximize $\hat{\theta}_d$ while minimizing $\hat{\theta}_f, \hat{\theta}_y$, i.e.:

$$(\hat{\theta}_f, \hat{\theta}_y) = \operatorname{argmin}_{\theta_f, \theta_y} E(\theta_f, \theta_y, \hat{\theta}_d), \tag{5}$$

$$\hat{\theta}_d = \operatorname{argmax}_{\theta_d} E(\hat{\theta}_f, \hat{\theta}_y, \theta_d). \tag{6}$$

DANN is able to cope with the lack of sufficiently large labeled target domain data by virtue of its good distributional alignment property for unlabeled target domain data. However, the prerequisite for DANN to work is to obtain enough unlabeled target domain samples for model training. When samples from the target domain are not available, $\frac{1}{n'}\sum_{i=n+1}^{N}\mathcal{L}_d^i(\theta_f, \theta_d)$ in Eq. (4) is missing, resulting in the inability of the DANN network to align the domain distribution of the data in the target domain, which severely reduces the effectiveness of the model on the target domain

3. Proposed Method

In exploring methods for domain generalization of bearing fault diagnosis, the main goal is to obtain bearing fault characteristics from the source domain that are invariant across different operating conditions. As highlighted in Section 2, the efficacy of traditional DANNs for generalization is greatly reduced due to the lack of target domain insight when target domain data is not available. To address this limitation, our study introduces a novel approach: a domain adversarial network enhanced with rationale invariant regularization, specifically tailored for cross-condition bearing fault diagnosis. The strength of this method lies in its dual approach.

During the backpropagation phase of our model's training, we focus on optimizing three pivotal objective functions. These include the sample label prediction loss and the rationale invariance loss, both pertaining to the label classifier, as well as the domain prediction loss associated with the domain discriminator. Each of these objective functions plays a vital role in refining the model's performance. The sample label prediction loss is instrumental in enhancing the accuracy of the model's fault type predictions, ensuring that the label classifier can correctly interpret and categorize the features extracted from the input data. The rationale invariance loss is equally crucial, as it helps in maintaining consistency across the rationale matrices for different fault categories, thereby bolstering the model's ability to generalize across diverse operational conditions. Lastly, the domain prediction loss is key to the effectiveness of the domain discriminator. It guides the discriminator in accurately identifying the operational domain of each data sample, a step essential for the model to adapt its learning to the specific characteristics of each domain. Together, the meticulous optimization of these three objective functions during backpropagation is essential for achieving a high degree of accuracy and generalizability in the final fault diagnosis model.

ISSN 2616-5767 Vol.7, Issue 4: 84-92, DOI: 10.25236/AJETS.2024.070413

The objective function of the label classifier consists of two parts: the sample label prediction loss and the rationale invariance loss. Given a sample from the source domain D_s^m and its corresponding label $\{x_i, (y_i = k)\}^m$, the label prediction loss can be expressed as:

$$\mathcal{L}_{cla}^i(\theta_f, \theta_y) = \mathcal{L}_{cla}(G_y(G_f(\mathbf{x}_i; \theta_f); \theta_y), y_i), \tag{7}$$

where G_f and G_y denote the deep feature extractor and label classifier, respectively.

The loss of rationale invariance, which is used to measure the difference between the rationale matrix of a sample and the rationale matrix of its corresponding category as a regularization term of the objective function, can be expressed as:

$$\mathcal{L}_{inv}^i = \sum_k || \mathbf{R}_i - \overline{\mathbf{R}}_k ||_2^2 \tag{8}$$

where $\|\bullet\|_2$ denotes the l2 paradigm, N_b is the number of samples in the batch in which the sample is located, R_i denotes the schema matrix of the *i*-th sample, and $\overline{R}_k$ denotes the average matrix of the k-th class of schema matrixes. From chapter 2.2.2 it is known that the independent variable $\mathbf{R}_i$ of $\mathcal{L}_{inv}^i$ is directly related to the parameter θ_f, θ_y of the feature extractor and label classifier, and $\overline{\mathbf{R}}_k$ is a constant matrix updated with $\mathbf{R}_i$, so it can be simplified and expressed as:

$$\mathcal{L}_{inv}^i \left(\theta_f, \theta_y, \overline{\mathbf{R}}_k\right) \tag{9}$$

4. Experimental Verification

In this section, we undertake a rigorous experimental validation of our proposed RIDAN-based cross-condition fault diagnosis method. This validation process utilizes two distinct bearing fault datasets: one from Guilin University of Electronic Technology and the other from Case Western Reserve University. These datasets provide a comprehensive platform to test and demonstrate the efficacy of our method under varied conditions. To ensure the reliability and reproducibility of our experiments, we have meticulously documented the software and hardware environments used. These details are systematically presented in Table 2. This table serves as a crucial reference, outlining the specific configurations and technical specifications of the environment in which our experiments were conducted. Such thorough documentation is essential for enabling other researchers to replicate our experimental setup and validate our findings independently. By providing this level of transparency, we aim to contribute to the robustness and credibility of the research in the field of fault diagnosis.

Table 2: Experimental Environment.

Software & Hardware	Version or Model
Python	3.10.4
Pytorch	1.13.1+cu117
Torchvision	0.14.1+cu117
NumPy	1.24.2
CUDA	11.7
CuDNN	8500
CPU	I7-13700KF
GPUs	Nvidia RTX 3090 Ti

4.1. Contrasting methods and layout details

To showcase the strengths of our proposed RIDAN-based method, we have selected several cutting-edge techniques in the field for comparative analysis.

To ensure a level playing field in our comparative analysis, we uniformly selected the Resnet34 network as the deep feature extractor for all methods under consideration. This choice facilitates a fair and consistent baseline for evaluating each method's performance. Additionally, for the training of the network, we employed the Stochastic Gradient Descent (SGD) optimizer, complemented by momentum

ISSN 2616-5767 Vol.7, Issue 4: 84-92, DOI: 10.25236/AJETS.2024.070413

and weight decay. This standardized approach to network training across all methods ensures that any observed differences in performance can be attributed more accurately to the inherent capabilities of each method, rather than variations in the underlying network architecture or optimization strategy. Such uniformity is crucial for conducting an unbiased and equitable comparison of these advanced fault diagnosis techniques. To ensure fine-tuning at the end of the training, the learning rate was chosen as a function of the decrease during learning, which is given by $\alpha = \alpha_0 / (1.0 + 10 * i)^{0.75}$, where α_0 denotes the initial learning rate and i denotes the percentage of iteration steps. The optimizer momentum for the proposed method m is set to 0.9. To be fair, the optimizer parameters for the comparison method are set the same as for the proposed method, and the rest of the hyperparameters use the default values from the original paper.

4.2. Case1 Guilin University of Electronic Technology Bearing Dataset

4.2.1. Introduction to the dataset

To rigorously validate the effectiveness of our proposed method in generalized fault diagnosis for cross-condition bearings, we have established a bearing fault simulation test bed. This setup is strategically located in the equipment diagnosis laboratory of Guilin University of Electronic Science and Technology. Utilizing this specialized test bed, we have meticulously collected and compiled a comprehensive bearing fault dataset. This dataset is instrumental in providing a realistic and controlled environment to assess the performance of our fault diagnosis approach, ensuring its applicability and reliability in practical, real-world scenarios.

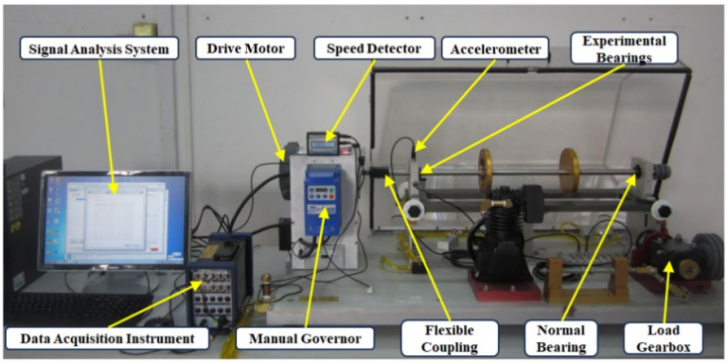

Figure 1:GUET Bearing Test Bench.

Figure 1 showcases the test rig utilized in our study, which was meticulously crafted by SpectraQuest, Inc., based in the United States. This test stand boasts a drive motor, equipped with both a manual speed governor and a speed detector. The drive motor is seamlessly connected to the spindle of our experimental setup via a flexible coupling. In our experiment's configuration, the faulty bearing was strategically mounted on the side adjacent to the drive motor, while the normal bearing was positioned on the opposite side. The spindle featured a diameter of 0.75 inches, and the specific faulty bearing model used in our experiments was the ER-12K. The motor's capacity was 1 HP. For data acquisition, a DH186 sensor was affixed to the test bench. This sensor was linked to a 16-channel portable data collector, the model VQ-USB16, enabling the transmission of data to the VQ data analysis system on a computer. This data collector is characterized by a maximum sampling frequency of 102.4 kHz and a bandwidth of 20 kHz. Further, detailed specifications of the ER-12K bearings are provided within the paper for comprehensive understanding.

Table 3: ER-12K Bearing Parameters.

Inside Diameter(mm)	Outside Diameter(mm)	Pitch Diameter(mm)	Number of Rolling Elements	Rolling Element Diameter(mm)	Contact Angle(°)
25.4	52	33.4772	8	7.9375	0

The manufacturing of the faults on the bearings, as depicted in Figure 2, was executed using the Electrical Discharge Machining (EDM) technique. This allowed for precise fault creation at various locations on the bearings. In addition to simulating a normal condition, we meticulously replicated a total of five types of bearing faults. These included inner race faults, outer race faults, rolling element faults, and composite faults (which encompassed a combination of issues in the inner race, outer race, and

ISSN 2616-5767 Vol.7, Issue 4: 84-92, DOI: 10.25236/AJETS.2024.070413

rolling elements), offering a robust and diverse set of scenarios for our fault diagnosis study.

Figure 2:Different Fault Types of GUET Dataset.

Bearing vibration data were collected under three different rotational frequency conditions (20Hz, 30Hz, 40Hz). The sampling frequency was 12.8 kHz and the acquisition time was 30 seconds.

4.2.2. Data preprocessing

For the GUET bearing dataset, we implemented a meticulous data preparation strategy. Each segment of the bearing signal was truncated to encompass the initial 153,600 data points. From this data, we generated gray-scale pixel images with a resolution of 32×32 pixels. Consequently, each of these images encapsulates 1,024 data points, offering a detailed and compact representation of the signal segment.

To ensure a comprehensive dataset, we converted each segment of the bearing signal into 150 gray-scale pixel images. These images serve as data samples for our analysis, providing a rich variety of signal representations. Figure 3 showcases exemplary images for different fault types, offering a visual insight into the diversity and complexity of the fault signatures captured in the dataset. This approach not only enhances the robustness of our dataset but also facilitates a more nuanced understanding and analysis of the bearing fault types, crucial for the accuracy and effectiveness of our fault diagnosis methodology.

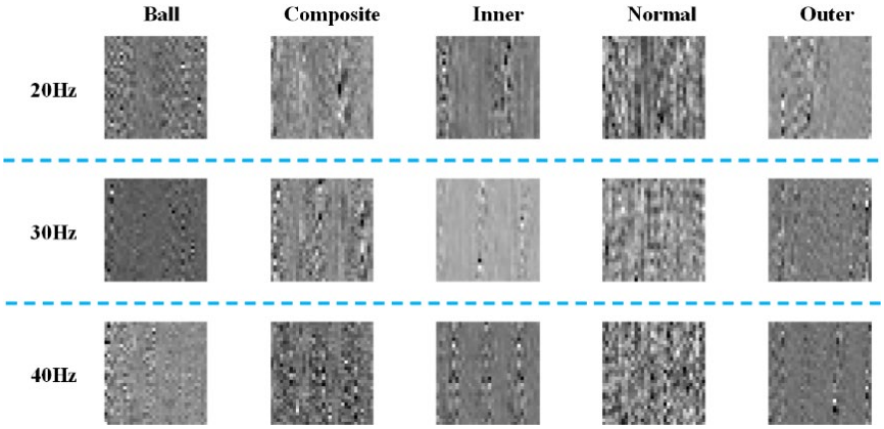

Figure 3:Gray Pixel Images of GUET Dataset.

4.2.3. Experimental Results and Analysis

The experiments are set up according to different rotation frequency domains. In each group of experiments, the dataset of one specific rotation frequency is set as the target domain, while the datasets of the other two rotation frequencies are used as the source domain. To simplify the presentation, G1, G2, and G3 are used in this paper to represent the classification tasks with different target rotation frequencies. For example, G1 refers to the source domain data with rotation frequencies of 30 Hz and 40 Hz, while the target domain data has a rotation frequency of 20 Hz. The number of data samples in the training set is calculated by the following formula: the number of gray pixel images for each fault type multiplied by the number of fault categories multiplied by the number of source domains. It is worth noting that during the model training phase, only the source-domain data are used for training the model, while the target-domain data are used only for testing the model's effectiveness. Each experiment is trained for 120 epochs.

1) Results

The accuracy and mean values of the proposed and compared methods are shown in Table 4.

ISSN 2616-5767 Vol.7, Issue 4: 84-92, DOI: 10.25236/AJETS.2024.070413

Table 4: Results of GUET Dataset.

Method	G1	G2	G3	average
Mixup	0.909333	0.978667	0.844	0.910667
SelfReg	0.912	0.982667	0.830667	0.908444
CORAL	0.9333	1	0.9027	0.945333
GroupDRO	0.9147	1	0.896	0.9369
RSC	0.9493	0.9987	0.9493	0.965767
ANDMask	0.944	0.9987	0.9187	0.9538
DIFEX	0.9427	0.9973	0.928	0.956
RIDAN	**0.964**	**1**	**0.972**	**0.978667**

Table 4 show the accuracy of the proposed method and all comparison methods on the G1-G3 task, in order to eliminate the influence of random factors, each experiment was repeated three times to take the average value as the final results. According to the experimental results, it can be seen that all the methods perform best on G2 and relatively poorly on G1 & G3.

In most of the domain generalization tasks, the proposed method shows superior and stable results compared to the other methods. Specifically, the present method outperforms the second-ranked MMD method by about 4% on average on all tasks. The results show that data augmentation-based domain generalization methods (e.g., Mixup and SelfReg) perform poorly when the domain distribution shift is large. We believe this may be due to the fact that data augmentation methods are unable to precisely control the direction or degree of augmentation, which leads to a degradation of the model's performance in the face of large distributional offsets. In contrast, domain invariant feature learning methods such as RSC and CORAL can better adapt to the data distribution of the target domain when the degree of distribution shift is large by focusing on learning invariant features within the domain.

2) Validity analysis:feature visualization and confusion matrix

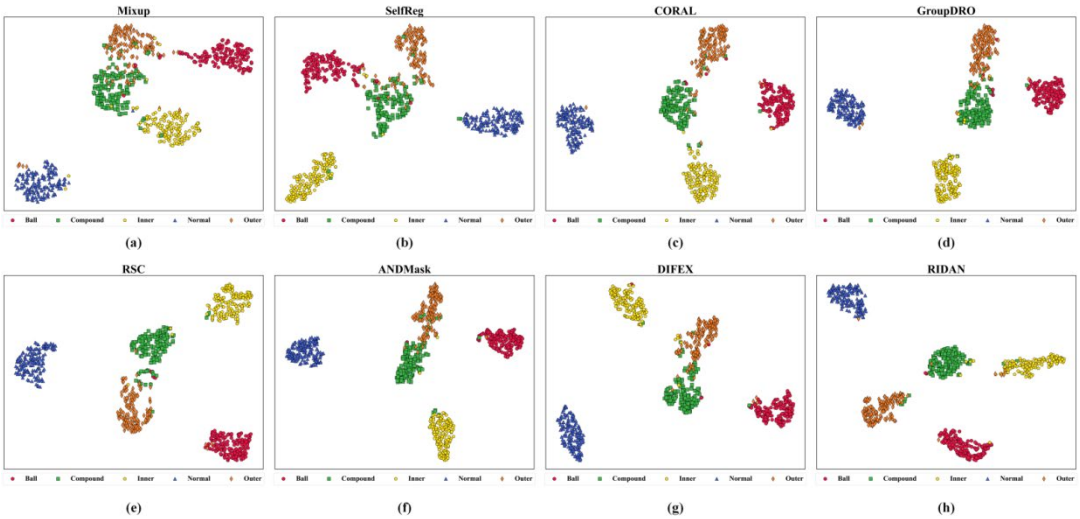

Figure 4: T-SNE Images of Different Methods in Case 1.

To evaluate the capability of the proposed methods in this paper in terms of learning features, we employ the t-SNE (t-Distributed Stochastic Neighbor Embedding) technique. t-SNE is a popular dimensionality reduction technique that effectively presents high-dimensional datasets in a two- or three-dimensional low-dimensional space, which facilitates visualization and analysis. Figure 4 shows the t-SNE image results of each method on the G1 task.

From these t-SNE images, we can observe that most of the methods perform poorly in recognizing composite faults, and these methods tend to confuse composite faults with other types of faults (especially outer ring faults). In contrast, the method proposed in this paper effectively learns and distinguishes features from various types of faults, showing clear classification boundaries between different classes of features in high-dimensional space. This result shows that our method excels in fault type identification and differentiation ability in high-dimensional feature space.

To further investigate the classification performance of the proposed methods, the confusion matrixes of different methods on task G1 are shown in Figure 5. The real fault types are represented by rows and the predicted fault types are represented by columns. The results of the confusion matrix are consistent with the t-SNE image, which verifies that the comparison method is less effective in feature learning for

ISSN 2616-5767 Vol.7, Issue 4: 84-92, DOI: 10.25236/AJETS.2024.070413

composite faults, while the proposed method is optimal in classifying all fault categories.

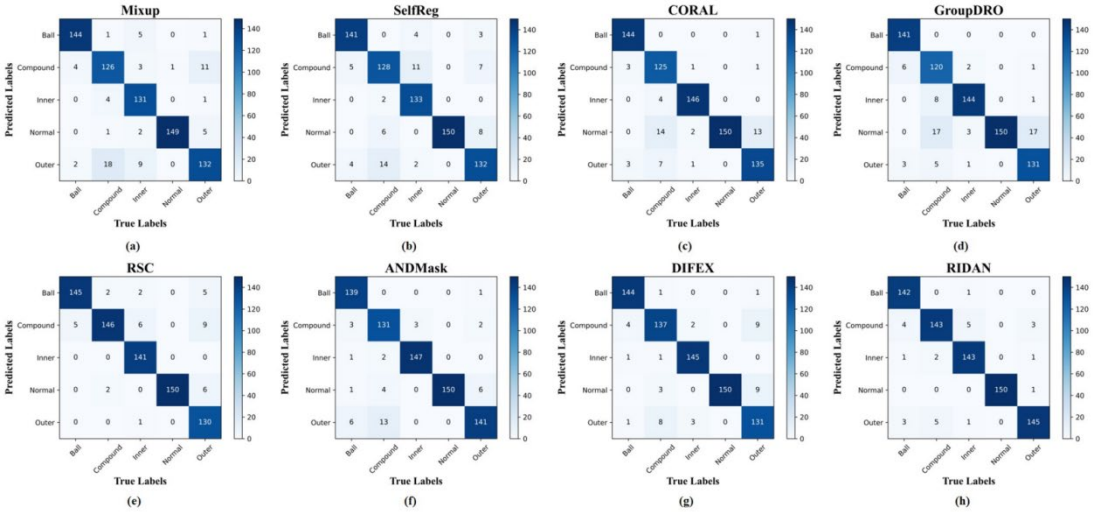

Figure 5:Confusion Matrix of Different Methods in Case 1.

5. Conclusion

To address the challenge of unavailable target operating condition bearing data in real-world production settings, we introduce an innovative cross-domain bearing intelligent fault diagnosis method based on the RIDAN network. This method leverages the principles of domain adversarial learning and domain generalization. It notably addresses the limitation of traditional DANN models, which tend to experience a decline in generalization ability in the absence of target-domain bearing fault data. This is achieved by incorporating a rationale invariant module within the label classifier. In this research, extensive experiments were conducted using both the GUET and CWRU bearing datasets, comparing our method against contemporary popular domain generalization approaches. These experiments robustly demonstrate the effectiveness and superiority of our proposed method. They confirm that our approach can adeptly facilitate intelligent fault diagnosis of bearings under varying degrees of distributional deviations, as evidenced across two different datasets. Additionally, the significant contribution of the rationale invariant regularization module to enhancing model performance is further substantiated through ablation studies. Despite these advancements, our method is not without its limitations. A key area of future research will focus on how to enhance the diagnostic model's performance in scenarios where multiple source domains may not comprehensively cover the data distribution of the target domain. This aspect represents a crucial frontier in our ongoing efforts to refine and improve our intelligent fault diagnosis methodologies.

Acknowledgments

The financial sponsorship from the project of Natural Science Foundation of Guangxi (Grant no. 2021GXNSFBA075050), It's also sponsored by Guangxi Key Laboratory of Manufacturing System & Advanced Manufacturing Technology, School of Mechanical and Electrical Engineering, Guilin University of Electronic Technology (Grant no. 20-065-40-004Z).

References

[1] X. Wang, H. Jiang, Z. Wu, Q. Yang, Adaptive variational autoencoding generative adversarial networks for rolling bearing fault diagnosis, Adv Eng Inform, 56 (2023) 102027.
[2] Z. Wang, J. Yang, Y. Guo, Unknown fault feature extraction of rolling bearings under variable speed conditions based on statistical complexity measures, Mech Syst Signal Pr, 172 (2022) 108964.
[3] Shuilong He, Qianwen Cui, Jinglong Chen, Tongyang Pan, Chaofan Hu. Contrastive feature-based learning-guided elevated deep reinforcement learning: Developing an imbalanced fault quantitative diagnosis under variable working conditions[J]. Mechanical Systems and Signal Processing, 2024, 211: 111192.

ISSN 2616-5767 Vol.7, Issue 4: 84-92, DOI: 10.25236/AJETS.2024.070413

[4] D. Zhao, S. Liu, H. Du, L. Wang, Z. Miao, Deep branch attention network and extreme multi-scale entropy based single vibration signal-driven variable speed fault diagnosis scheme for rolling bearing, Adv Eng Inform, 55 (2023) 101844.
[5] P. Lyu, K. Zhang, W. Yu, B. Wang, C. Liu, A novel RSG-based intelligent bearing fault diagnosis method for motors in high-noise industrial environment, Adv Eng Inform, 52 (2022) 101564.
[6] X. Li, Y. Yang, N. Hu, Z. Cheng, H. Shao, J. Cheng, Maximum margin Riemannian manifold-based hyperdisk for fault diagnosis of roller bearing with multi-channel fusion covariance matrix, Adv Eng Inform, 51 (2022) 101513.
[7] A. Rai, S.H. Upadhyay, A review on signal processing techniques utilized in the fault diagnosis of rolling element bearings, Tribol Int, 96 (2016) 289-306.
[8] J. Lu, B. Jia, S. Li, S. Gong, A noise reduction method of rolling bearing based on empirical wavelet transform and adaptive time frequency peak filtering, Meas Sci Technol, 34 (2023) 125146.
[9] J. Zheng, S. Huang, H. Pan, J. Tong, C. Wang, Q. Liu, Adaptive power spectrum Fourier decomposition method with application in fault diagnosis for rolling bearing, Measurement, 183 (2021) 109837.
[10] S. Aziz, M.U. Khan, M. Faraz, G.A. Montes, Intelligent bearing faults diagnosis featuring Automated Relative Energy based Empirical Mode Decomposition and novel Cepstral Autoregressive features, Measurement, 216 (2023) 112871.
[11] Z. Liu, D. Peng, M.J. Zuo, J. Xia, Y. Qin, Improved Hilbert–Huang transform with soft sifting stopping criterion and its application to fault diagnosis of wheelset bearings, Isa T, 125 (2022) 426-444.
[12] J. Wang, C. Lan, C. Liu, Y. Ouyang, T. Qin, W. Lu, Y. Chen, W. Zeng, P. Yu, Generalizing to Unseen Domains: A Survey on Domain Generalization, IEEE Transactions on Knowledge and Data Engineering, (2022) 1-1.